Remote Sensing of Environment 235 (2019) 111433

Contents lists available at ScienceDirect

Remote Sensing of Environment

journal homepage: www.elsevier.com/locate/rse

A multi-frequency framework for soil moisture retrieval from time series radar data

Liujun Zhu[a,b,*], Jeffrey P. Walker[a], Leung Tsang[b], Huanting Huang[b], Nan Ye[a], Christoph Rüdiger[a]

[a] Department of Civil Engineering, Monash University, Clayton, Vic. 3800, Australia
[b] Department of Electrical Engineering and Computer Science, Ann Arbor, MI, 48109-2122, USA

ARTICLE INFO

Keywords:
Multi-temporal
Soil moisture
Multi-frequency
Synthetic aperture radar

ABSTRACT

The increased availability of spaceborne radar data projected over the next decade provides a great opportunity for operational soil moisture mapping with high spatial (< 50 m) and temporal (< 3 days) resolution, by combining the data from multiple SAR missions. Accordingly, a multi-frequency soil moisture retrieval framework has been proposed, being applicable for SAR missions operating at the commonly used remote sensing frequencies of L-, C- and X-band. A combination of numerical, physical and semi-empirical scattering models was selected to build a series of forward modeling look up tables (LUTs) covering the typical radar configurations and nature surface conditions. An unsupervised change detection method was integrated to identify areas with abrupt roughness and vegetation changes, so that time-series data collected from different SARs can be combined with the assumption of time-invariant roughness and vegetation. The multi-frequency backscattering coefficient (σ^0) with negligible scattering from soil surface (equivalent to calibration uncertainty) was then removed before soil moisture retrieval. Finally, soil moisture retrieval was carried out independently for each landcover type using an optimization method and forward LUTs. Evaluation based on the Soil Moisture Active Passive Experiment-5 dataset consisting of L-band airborne data, C-band RADARSAT-2 data and X-band COSMO-SkyMed data showed an acceptable overall root mean square error (RMSE) of 0.058 cm^3/cm^3 at the paddock scale (~0.1 – 0.5 km). The comparison with single and dual frequency retrieval suggests that multi-frequency retrieval is not necessary to have the highest accuracy. However, it is still valuable to joint use multi-frequency data consider the limited deterioration in accuracy and the significantly enhanced temporal resolution.

1. Introduction

The validity of synthetic aperture radar (SAR) data for soil moisture retrieval has been demonstrated at high spatial resolution using commonly used remote sensing frequencies, i.e., L- (Kim et al., 2012a; Ouellette et al., 2017; Shi et al., 1997; Zhu et al., 2019a), C- (Balenzano et al., 2011; Bousbih et al., 2017; Satalino et al., 2002) and X-band (Aubert et al., 2011; Bai et al., 2015; El Hajj et al., 2016). The temporal resolution of a single SAR mission is, however, insufficient for the 1–5 days repeat requirement of most applications (Engman, 1992; Jackson et al., 1999; Walker and Houser, 2004). Several satellite constellations have recently been launched or proposed, having an enhanced global revisit of ~ 1 week, e.g., the C-band Sentinel-1 (6 days) and L-band SAOCOM (8 days). The combination of these constellations together with the irregular observations of other radars, e.g., the L-band PALSAR-2, C-band RADARSAT-2 and X-band COSMO-SkyMed, provide a great opportunity for soil moisture mapping with high spatial (< 50 m) and temporal resolution (< 3 days).

Despite the great promise that this integrated approach provides, joint soil moisture retrieval from multiple SAR missions can be more complex than those from a single data source, because of the irregular observations of multiple SAR missions in time and their inconsistent radar configurations (frequency, incidence angle and polarization). Multi-configuration is widely acknowledged as a merit in soil moisture retrieval, because they respond differently to geophysical parameters and can thus help to separate the effect of soil moisture from others (Kornelsen and Coulibaly, 2013; Ulaby et al., 2014). Multi-frequency also potentially allows to capture the geophysical details in the vertical because of the increased penetration through the canopy and increased penetration depth in the soil at longer wavelengths (Moghaddam et al., 2000). However, accurate forward modeling for various radar configurations is still a challenge. Commonly used scattering models for bare soil surface include: i) the semi-empirical Dubios model (Dubois et al., 1995), Oh model (Oh, 2004); ii) the physical based Integrate Equation

* Corresponding author. Department of Civil Engineering, Monash University, Clayton, Vic. 3800, Australia.
E-mail address: liujun.zhu@monash.edu (L. Zhu).

https://doi.org/10.1016/j.rse.2019.111433
Received 19 June 2019; Received in revised form 30 August 2019; Accepted 19 September 2019

Model (IEM; Fung, 1994); and iii) numerical solutions of Maxwell's question in three demission (NMM3D; (Huang et al., 2017a; Huang and Tsang, 2012; Tsang et al., 2017). An additional vegetation scattering model, e.g., the water cloud model (Attema and Ulaby, 1978), distorted Born approximation (DBA; Lang and Sighu, 1983) or radiative transfer (RT) models (Ulaby et al., 1990), is required for vegetated areas. Limited by their validity ranges, one model can hardly cover the potential remote sensing radar configurations and land surface conditions. For instance, the maximum root mean square height is ~ 1 cm for X-band in the IEM (Fung, 1994), which cannot capture the range of potential geophysical values. Moreover, the IEM tends to have larger discrepancy with measurements at larger incidence angles (Mancini et al., 1999). While empirical or semi-empirical relationships (e.g., Baghdadi et al., 2016) based on multiple campaigns may work well, they still suffer from cumbersome configuration-specific parameter tuning, especially for vegetated areas. Recent developments of machine learning methods (especially the artificial neural network, ANN) and the coming big SAR data, provide a promising data-driven alternative (Mirsoleimani et al., 2019; Paloscia et al., 2008; Pasolli et al., 2015). However, a robust deep ANN with satisfactory generalization capability requires a huge amount of ground soil moisture sampling that are not readily available.

Soil moisture retrieval from multi-configuration data implies an inverse processing of these models which is an ill-posed problem when using single configuration data (Kornelsen and Coulibaly, 2013). Two categories of methods are encountered in literature in view of time instances, i.e., snapshot methods and multi-temporal methods. The snapshot methods produce soil moisture values of a time slice (a date or period with assumed constant geophysical parameters), which is commonly directly inverted from multi-polarization (e.g., McNairn et al., 2012; Mirsoleimani et al., 2019; Oh, 2004), multi-angular (e.g., Notarnicola et al., 2008; Shen et al., 2013; Srivastava et al., 2009; Zribi and Dechambre, 2003) and/or multi-frequency data (Bindlish and Barros, 2000, 2001; Pierdicca et al., 2008; Zhang et al., 2018). The retrieved soil moisture or roughness values in previous time instances are sometimes treated as *a prior* information for the subsequent retrieval (Joseph et al., 2008; Rahman et al., 2008; van der Velde et al., 2012), although the risk for sharing roughness values among different frequency or incidence angles has been reported in several studies (Baghdadi et al., 2004; Lievens et al., 2011). Despite the promising performance of these snapshot methods, it is quite inconvenient for soil moisture retrieval from multiple SAR missions, because multiple snapshot algorithms are required to deal with the irregular observations acquired at different time instances.

In contrast, multi-temporal methods retrieve time series soil moisture collectively from time series SAR data, based on the assumption of time-invariant roughness and vegetation parameters over the given time window. The rational of the assumption is that surface roughness, and vegetation parameters undergo relatively slower temporal transitions in comparison to soil moisture, excluding cultivation practices (Balenzano et al., 2011; Kim et al., 2012a). The difference/ratio of multi-temporal SAR observations can therefore be directly related to a soil moisture value or index (Balenzano et al., 2011; Notarnicola, 2014; Ouellette et al., 2017; Wagner et al., 1999; Wickel et al., 2001). The assumption can also be used to remove the major part of unknowns representing the time-variation surface roughness and vegetation in the inversion of forward scattering models (Kim et al., 2014a; Kim et al., 2012a; Kim and Van Zyl, 2009; Kweon and Oh, 2014; Mattia et al., 2009; Pierdicca et al., 2010). These methods commonly require consistent radar configuration of the input data, being not suitable for joint soil moisture retrieval from multiple SAR missions.

In our previous study (Zhu et al., 2019a), a time series multi-angular method was proposed for joint soil moisture retrieval from multiple L-band SAR missions. Here, that method was extended to include multi-frequency data. The capability of L-band for soil moisture retrieval over densely vegetated areas has been widely acknowledged (El Hajj et al., 2019; Kim et al., 2017; Zribi et al., 2019), with the effectiveness of shorter wavelengths (C- and X-band) requiring further investigation. A number of studies have reported the considerable sensitivity of C band (~5.4 GHz; Sentinel-1, RADARSAT-2) to soil moisture over densely vegetated areas, especially for small incidence angles (Balenzano et al., 2011; Bousbih et al., 2017; Brown et al., 2003; Toure et al., 1994). Despite the higher attenuation, several studies have also suggested that X-band can be effective for soil moisture retrieval over dense grass (Aubert et al., 2011; El Hajj et al., 2016). In addition, the HH polarization commonly has a higher sensitivity than VV for vegetation areas dominated by vertical structures (Balenzano et al., 2011; Bindlish and Barros, 2001; Ulaby et al., 2014). These results have important implications for selecting the radar data to be used in soil moisture retrieval, but are still not straightforward for determining whether a backscattering measurement contains reliable information of soil moisture. Consequently, a model-based method was developed to determine the effectiveness of a given radar measurement as a step of the proposed framework.

Multi-angular forward look up tables (LUTs) for L-band built by NMM3D and DBA (Zhu et al., 2019a) were extended to cover C-band (5.4 GHz) and X-band (9.3 GHz) using the Oh model (Oh et al., 1992) and DBA (Lang and Sighu, 1983). In addition, the change detection method proposed in Zhu et al. (2019b) was integrated to ensure the assumption of time-invariant roughness and vegetation. The proposed framework was evaluated using the time series multi-frequency data collected during the fifth Soil Moisture Passive Active Experiment (SMAPEx-5) consisting of L-band airborne data, C-band RADARSAT-2 data, X-band COSMO-SkyMed data and extensive ground observations. The effect of frequency combinations on retrieval accuracy were also investigated to guide the use of the method in future applications. The novelty of the proposed method is that i) it provides a general retrieval framework for multiple forthcoming SAR missions, providing an alternative approach to mapping soil moisture with high spatial (< 100 m) and temporal (< 3 days) resolutions, and ii) it provides a way to combine multi-temporal data from irregularly collected multi-frequency observations for soil moisture retrieval.

2. The proposed framework

2.1. Overview of the framework

Fig. 1 outlines the proposed framework. Inputs include the landcover of the research area and time series radar data from three platforms (but not limited to those platforms). The framework starts from the construction of forward modeling LUTs, covering the commonly used configurations in radar remote sensing, and the range of soil roughness, soil moisture and vegetation water content (VWC). The time series data was first used to detect the potential roughness and VWC changes caused by cultivation activities and rainfall events. Time series with detected changes were then separated into multiple sub-series accordingly, ensuring the assumption of time-invariant roughness and vegetation. Soil moisture retrieval was then carried out independently on each sub-series. For the vegetated area, the relative backscatter contribution relating to that from the soil surface (C_s) was calculated using the forward models. Radar data with negligible (equivalent to the data calibration uncertainty) soil contribution was removed before soil moisture retrieval. Finally, soil moisture retrieval was carried out independently for each landcover type using an optimization method and LUTs.

Steps 1 and 2 in Fig. 1 can be treated as pre-processing stages of the soil moisture retrieval, which are designed to ensure the assumptions of the method are met and that the radar measurements without sufficient soil information have been removed, respectively. The details of the method used in step 1 can be found in Zhu et al. (2019b). Briefly, the time series ratio of HV, the temporal difference of HV/VV, and the temporal difference of VV polarizations were first calculated at the paddock scale. The Density-Based Spatial Clustering of Applications

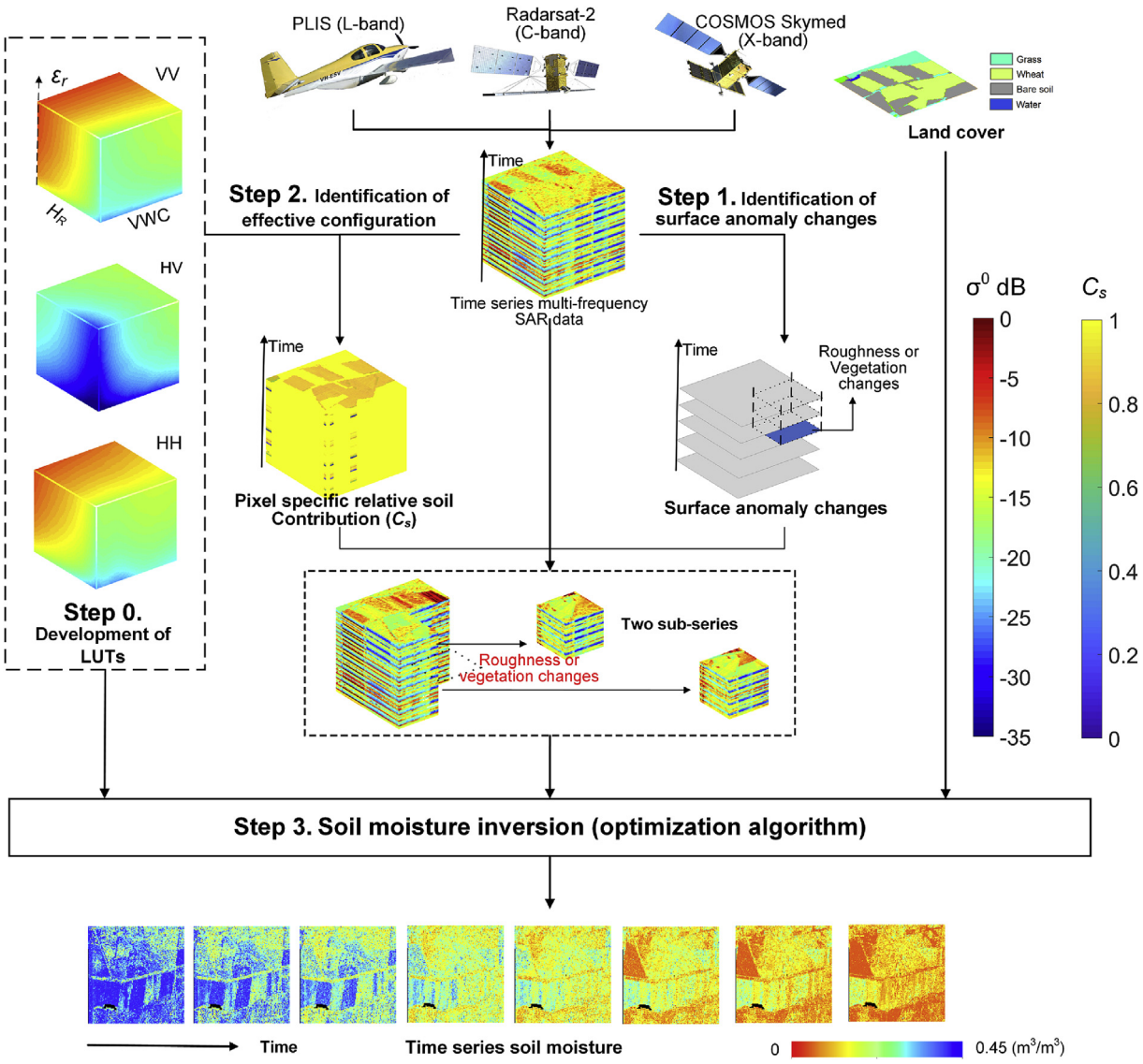

Fig. 1. Conceptual framework of the proposed time series multi-frequency retrieval method. The inputs include time series L-, C- and X-band data acquired from both ascending and descending orbits; the landcover map, and the forward data cubes (multi-dimensional look up tables).

with Noise (DBSCAN) method was then applied to identify the potential changes of each time slot, and refined using the time series results. The other steps are as follows.

2.2. Scattering models and forward LUTs

In our previous study (Zhu et al., 2019a), NMM3D was used to simulate the L-band (1.26 GHz) backscattering coefficient (σ^0) and coherent reflectivity over a range of directionally isotropic bare soil surface. Considering the limited sensitivity of soil moisture retrieval to the correlation length, except for very rough surfaces (Kim et al., 2012a; Oh et al., 2002; Shi et al., 1997), the bare surfaces were characterized in terms of root mean square height (H_R), the real part of the relative permittivity (ε_r) and a fixed correlation length (L_C) of $10H_R$ (Zhu et al., 2019a). The theory of DBA was applied to model the σ^0 over vegetated area. The required vegetation parameters (e.g., density and length of vegetation particles) were related to a single vegetation parameter of vegetation water content (VWC), through allometric relationships and ground measurements (Zhu et al., 2019a). To avoid numerical or analytical inversion, land cover specific look up tables (LUT) were built as the forward representation of scattering models at L-band.

These LUTs were extended to cover the C-band (5.4 GHz) and X-band (9.3 GHz) here. Since the H_R of available NMM3D simulations for all incidence angles is limited to 0.168 of the wavelength (Huang et al., 2010), it is applicable for the H_R value up to only ~ 0.93 and 0.54 cm for C- and X-band respectively. Some simulation cases for larger H_R values are available in Liao et al. (2016). However, they are still insufficient to cover the range (0.5 – 5 cm) of a typical soil surface (Jackson et al., 1997; Oh et al., 1992; Zribi et al., 2014a). Consequently, the Oh model (Oh et al., 1992) was used to model the σ^0 of soil surface at C- and X-band because of its large validity range. Similar to the assumptions made for the NMM3D simulations at L-band, the soil surface training data used for the Oh model also followed a stationary Gaussian random process with directionally isotropic correlation functions (Oh et al., 1992). This is not easily satisfied for agriculture areas with directional row or tillage features. Consequently, effective isotropic roughness values were assumed for these areas as suggested in several studies (Champion and Faivre, 1996; Joseph et al., 2010; Zhu et al., 2019a). In line with the LUTs for L-band (Zhu et al., 2019a), H_R was selected as the only independent effective roughness parameter to account for the effect of a complex soil surface at C- and X-band. The corresponding L_C required in the Oh model was also determined by a

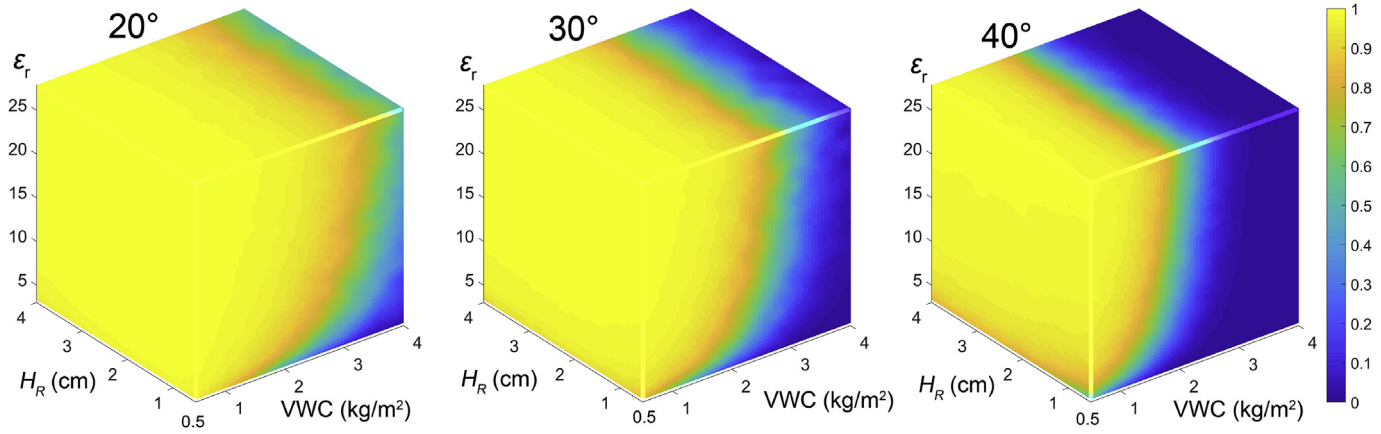

Fig. 2. Relative contributions related to the soil surface (C_s) for wheat at C-band VV polarization with incidence angles from left to right being 20°, 30° and 40°.

fixed L_C/H_R ratio of 10, considering 1) the need to be consistent with the L-band LUT for joint soil moisture mapping from multi-SAR missions, 2) the limited sensitivity of the L_C/H_R ratio in the Oh model (Oh, 2004) and 3) the negligible forward improvement (< 0.2 dB) using calibrated L_C values in the Oh model at the same research area (Panciera et al., 2014).

The DBA used for L-band LUTs first assumed that the wave incident on each vegetation scatterer is the mean field in the vegetation layer, and the mean scattered fields then computed by embedding the scatterers in the equivalent medium (Lang and Sighu, 1983). The assumption is valid when the scatterers have a small albedo, which holds for frequencies up to 10 GHz for plant canopy (Moghaddam and Saatchi, 1995). Accordingly, the DBA was directly used for C- and X-band. The three dominant contributions in the DBA can be expressed as (Lang and Sighu, 1983):

$$\sigma^0_{pq,v} = dQ_{pq,d}\frac{1 - e^{-(\tau_p+\tau_q)}}{\tau_p + \tau_q} \tag{1}$$

$$\sigma^0_{pq,db} = dQ_{pq,sr}R_p e^{-(\tau_p+\tau_q)} + dQ_{pq,rs}R_q e^{-(\tau_p+\tau_q)} \tag{2}$$

$$\sigma^0_{pq,s} = \sigma^0_{pq,g} e^{-(\tau_p+\tau_q)}, \tag{3}$$

where subscripts *v*, *db* and *s* are the volume, double-bounce and surface scattering, respectively. Subscripts *q* and *p* are either horizontal (H) or vertical (V). The quantities *Q* in Eqs. (1) and (2) are the backscattering cross section per unit depth of vegetation layer, with the subscripts *d*, *sr*, *rs* denoting the direct scattered, scattered-reflected and reflected-scattered scattering, while τ_p is the optical depth of the layer for the polarization *p*; both *Q* and τ vary according to specific geometric and dielectric properties of the discrete scatterers. The ground backscattering coefficient $\sigma^0_{pq,g}$ is calculated using the Oh model (Oh et al., 1992). The remaining quantity R_p is the reflectivity of ground surface for polarization *p*, which is calculated using Kirchhoff's technique (Ulaby et al., 2014):

$$R_p = |\rho_p|^2 \exp(2k_0 H_R \cos\theta) \tag{4}$$

where k_0 is the free-space propagation constant, θ is the angle of the incident wave, and ρ_p is the Fresnel reflection coefficient at the polarization *p*.

Similar to the L-band LUTs, the H_R and VWC of C- and X-band LUTs ranged from 0.5 to 4 cm and 0.5 – 4 kg/m^2, respectively. Please refer to Zhu et al. (2019a) for the geometric and dielectric properties of the discrete scatterers within the vegetation layer and their relationship with VWC. Different soil ε_r were used for C- and X-band LUTs to have a roughly consistent soil moisture range (0.03–0.43 m^3/m^3). LUTs for bare soil were generated directly using the Oh model with 256 equal grids for H_R and ε_r and 31 equal incidence angles ranging from 20 to 50°. The initial LUTs for a vegetated area were generated with a VWC resolution of 0.05 kg/m^2 at seven incidence angles, ranging from 20° to 50° with an interval of 5°. These were then interpolated into 31 incidence-angle-specific cubes (256 × 256 × 256), with the three dimensions being H_R and ε_r and VWC respectively. The error caused by the interpolation was less than 0.05 dB.

2.3. Determination of effective radar configuration

As no straightforward method for determining the effective radar configuration could be found in literature, a quantitative method was presented here. The basis of the method is that when the backscattered signal related to the soil surface falls below a certain level it is no longer making a detectable contribution to the total returned signal. Such a radar measurement may therefore only contribute noise in the soil moisture retrieval. Specifically, the effectiveness of a radar measurement in linear units is determined by:

$$\frac{\sigma^0_s + \sigma^0_{db}}{\sigma^0_v + \sigma^0_s + \sigma^0_{db}} \geq \partial\sigma^0_{all}(m_v, E_{cal}), \tag{5}$$

where the left and right sides are the relative contribution related to the soil (C_s) and the sensitivity of backscatter ($\partial\sigma^0_{all}$) to soil moisture (m_v) and calibration accuracy (E_{cal}), respectively. For a 0.02 m^3/m^3 change of soil moisture, the corresponding backscattering coefficient changes can be 0.15–1 dB depending on radar configurations and soil properties (Altese et al., 1996). The absolute radiometric calibration is commonly on the order of 1 dB (Christensen et al., 1998; Shimada et al., 2009; Zhu et al., 2018). Therefore, a sensitivity of 1 dB was considered as being appropriate, yielding a ratio of ~0.23.

The volume, double bounce and soil surface scattering in Eq. (5) can be determined by Eqs. (1)–(3) with the knowledge of VWC, H_R and soil moisture. This is, however, impractical for real applications as these geophysical parameters are those to be determined. Fig. 2 shows, as an example, the C_s of wheat at C-band VV polarization generated by the forward model. As expected, VWC was the dominant parameter, while H_R and ε_r were insensitive to C_s. Hence, given the radar frequency, incidence angle and polarization, an initial guess of VWC is probably to be sufficient for determining C_s. Accordingly, the VWC of each gird was estimated using the radar vegetation index (RVI; Kim and Van Zyl, 2009):

$$\mathrm{RVI} = \frac{8\sigma^0_{HV}}{\sigma^0_{HH} + \sigma^0_{VV} + 2\sigma^0_{HV}} \tag{6}$$

RVI is a sensitive indicator of biomass and VWC, with several empirical relationships between VWC and RVI available in literature (Huang et al., 2016; Kim et al. 2012b, 2014b). To consider the vegetation condition in the whole retrieval period, all available full-polarized radar data were used to calculate the RVI and then the average

VWC over time of each pixel was estimated using the empirical relationships. The average relative soil contribution (C_s) of each input radar measurement (σ^0) was subsequently determined from the corresponding soil contribution LUTs. For instance, given a σ^0 (C-band VV polarization; $\theta = 30°$) with an estimated VWC of 2 kg/m^2, the average C_s can be determined from the middle cube of Fig. 2 by averaging the slice corresponding to the VWC of 2 kg/m^2. Radar measurements with an average C_s less than 0.23 were removed before soil moisture retrieval. It is worth noting that the estimated VWC here is not used in the soil moisture retrieval.

2.4. Multi-frequency retrieval method

The time series multi-angular retrieval algorithm proposed in Zhu et al. (2019a) was extended for multi-frequency data. Radar data with the same acquisition date was treated as data collected simultaneously. Given a time series acquired at N dates with the ith date containing M_i multi-configured channels or independent σ^0 measurements, the soil moisture retrieval is a searching process to minimize the cost function between simulated and observed σ^0:

$$f = \frac{X(\varepsilon_{r,1}, \varepsilon_{r,2}, \ldots, \varepsilon_{r,N})}{N} \sum_{i=1}^{N} \sqrt{\frac{1}{M_i} \sum_{j=1}^{M_i} w_{ij} \cdot (\sigma_{ij}^0 - \sigma_{\mathrm{LUT},ij}^0(s, \varepsilon_{r,i}, VWC))^2}, \quad (7)$$

where $\sigma_{\mathrm{LUT},ij}^0(s, \varepsilon_{r,i}, VWC)$ and σ_{ij}^0 are backscattering coefficients from the LUT and observation in dB respectively, with the subscript i and j being the time index and the order of available channels on the ith date. The weight w_{ij} was set as a uniform value of 1 because of the difficulty to model the speckle noise, the differing error of forward models and calibration at different channels (Zhu et al., 2019a). The assumption of a monotonic dry down in the time series, proposed in Zhu et al. (2019a) as a constraint to partly remove the effect of random fluctuations over time, was also used here. However, this assumption is directly integrated into the cost function as

$$X(\varepsilon_{r,1}, \varepsilon_{r,2}, \ldots, \varepsilon_{r,N}) = \sum_{i=1}^{N} |k_i - i| + 1, \quad (8)$$

where k_i is the order of $\varepsilon_{r,i}$ in the relative permittivity series. X has a minimum value of 1 for a non-increasing relative permittivity series, while the maximum value is either $0.5(N^2+1)$ (N is odd) or $0.5N^2+1$ (N is even) for a strictly increasing series. A genetic algorithm was used to find the optimal solution of Eq. (6), with N permittivity values, one time-invariant H_R and VWC value retrieved simultaneously. A dielectric model presented in Dobson et al. (1985) converts the estimated dielectric constants into soil moisture.

3. Data sets

3.1. Ground measurements

The dataset used in this study was collected during the three-week SMAPEx-5. This campaign was carried out in Australia during spring (September 7–27, 2015) in the Yanco agricultural area (latitude 34°40.23′ S to 35°0.76′ S; longitude 145°58.84′ E to 146°21.28′ E). Yanco is a flat semi-arid agricultural and grazing area located in the Murrumbidgee River basin, Australia. A brief introduction is provided below with the detail being presented in Ye et al., 2016. Three SMAPEx-5 (YA4, YA7 and YE) focus farms were selected in this study (Fig. 3). YA4 and YA7 are characterized by cropping land use with the main landcover being wheat, grass, bare soil and openwood land, while YE is a grazing area with 80% of the area covered by grass. For analysis at the paddock scale, the boundaries of a few paddocks were delineated using visual-interpretation, being nearly half of selected area (Fig. 3). Specifically, grass paddocks were homogeneous patches with roughness and vegetation samples. Several open wood land paddocks were also selected and treated as grass land considering the small tree coverage (< 5%). Soil cultivation practices and irrigation were observed in SMAPEx-5 at four bare soil paddocks (#2, 30, 48 and 54) and six wheat paddocks (#72, 103, 109, 110, 115, and 116), respectively.

Extensive ground sampling of the top 5 cm soil moisture was carried out within the 3 focus farms shown in Fig. 3 on eight days during SMAPEx-5 (September 9th, 11th, 14th, 17th, 19th, 22th, 24th and 27th). Measurements were made using a portable sensor (Merlin et al., 2007) on a north-south oriented grid, with a spacing of 250 m. At each sampling location, small scale variation of soil moisture was captured using three point-based soil moisture measurements. A moderate rainfall occurred before the experiment followed by a drying down period, resulting in a wide range of soil moisture (0.04 – 0.45 m^3/m^3).

Soil profiles were measured at 2–3 locations within each selected paddock using a pin profiler between the soil moisture sampling dates. At each location, measurements were made in two orthogonal 3-m long segments, being north-south and east-west or along and across rows in the presence of row structures. The H_R and L_C of each 3 m-long surface height profile were derived from digital photographs. Measurements for paddocks with an isotropic surface were then averaged with the values labeled in Fig. 3. For those with periodical tillage features, H_R and L_C were averaged along and across rows respectively; also displayed in Fig. 3. In general, wheat and bare soil paddocks had a wide range of roughness with the large values observed on those with furrows due to tillage. Repeat measurements were also made in several selected paddocks (#2, #48, #55, #105, #161) with limited changes in time, excluding those with cultivation activities (Zhu et al., 2019b).

Intensive vegetation sampling, including plant size, geometry, and vegetation water content (VWC), was carried out over grass and wheat paddocks on a weekly basis; the available VWC measurements of each week are presented in Table 1. Relatively stable VWC was observed over the three-week campaign, with the temporal variation ascribed to the destructive collection of samples and the large intra-paddock heterogeneity (Zhu et al., 2019a). Consequently, the vegetation parameters were assumed constant in time with the collected data averaged for each paddock, and the average VWC of each paddock listed in Table 1.

3.2. Radar data

Twenty images collected at fifteen different dates of the three-week campaign were used in this study, covering the commonly used remote sensing frequency bands, i.e., 1.26 GHz (L-band), 5.4 GHz (C-band) and 9.3 GHz (X-band). The L-band data were acquired concurrently with the eight soil moisture sampling dates, using the airborne Polarimetric L-band Imaging SAR (PLIS) from south to north (ascending) and north to south (descending). PLIS is a fully polarimetric radar with incidence angles ranging from approximately 15°–50°, across an ~2.8 km swath in SMAPEx-5. The single look complex (SLC) PLIS data had a spacing of 2 m × 3.75 m. Please refer to Zhu et al. (2018) for details.

The C-band data set includes four RADARSAT-2 dual-polarization SLC acquisitions and three wide-swath quad-polarization SLC products, with varying incidence angle of 22°–40°. The slant range spacing is either 8 or 11.8 m, with a coincident azimuth spacing of 5.1 m. Two interferometric subsets of the COSMO-SkyMed (CSK) STRIPMAP HIMAGE (X-band) were available, with the ascending and descending subsets being collected by CSK-2 and CSK-1, respectively. The spacing of these SLC products is 3 m in both ground range and azimuth. A summary of those images is provided in Table 2, including the acquisition day of year (DOY), pass direction, frequency and polarization. All images were multi-looked and re-sampled to a pixel size of 25 m. A Landsat 8 pan-sharpening image was then used as the base for co-registration. The root mean square error (RMSE) of co-registration was less than 10 m.

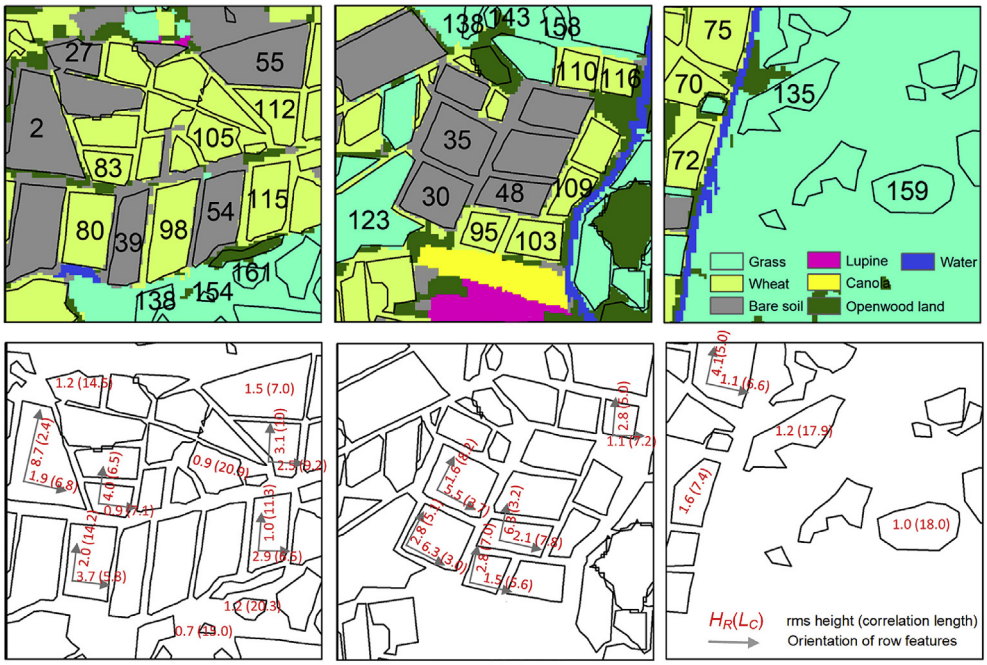

Fig. 3. Landcover and paddock numbers of three focus farms (top) in SMAPEx-5 with available roughness (bottom) paddocks in terms of H_R and L_C in units of cm. Soil roughness was measured in along and across the rows (the arrows in the bottom panel) for these with periodic features.

Table 1
Available vegetation water content measurements (kg/m^2) for the SMAPEx-5 focus farms used in this study.

#	Type	Week 1	Week 2	Week 3	SMAPEx-5
70	Wheat	–	2.28	1.91	2.00
72	Wheat	2.52	2.63	3.05	2.78
75	Wheat	3.31	2.55	2.94	2.93
80	Wheat	1.85	2.50	2.28	2.21
83	Wheat	3.11	–	–	3.11
95	Wheat	2.42	2.54	2.48	2.48
98	Wheat	–	–	2.69	2.69
103	Wheat	2.80	2.84	–	2.82
109	Wheat	1.89	2.18	2.87	2.32
110	Wheat	0.90	1.33	1.25	1.17
112	Wheat	1.59	1.35	1.90	1.60
115	Wheat	3.45	4.02	3.64	3.72
117	Wheat	2.71	3.21	–	2.93
135	Grass	0.55	0.83	0.70	0.69
138	Grass	0.73	–	–	0.73
143	Grass	1.47	1.69	1.68	1.62
154	Grass	1.22	–	–	1.22
158	Grass	0.92	–	–	0.92
159	Grass	–	0.53	–	0.53
161	Grass	0.70	1.24	0.99	0.98

-: not available.

4. Results

4.1. Evaluation of forward model

Backscattering coefficients (σ^0 in dB) were calculated at the paddock scale using the forward models (LUTs), ground measured H_R and VWC, which were compared with the radar observations in Fig. 4. Overestimations of 2–4.5 dB for C-band were observed over bare soil using the Oh model, in line with similar results observed in several previous studies ranging from 1 - 5 dB (Baghdadi and Zribi, 2006; Choker et al., 2017; Merzouki et al., 2010). While the available database is not large enough for a detailed study to analyze the behavior of forward accuracy as a function of incidence angle at C- and X-band, the angular dependence of forward accuracy was not observed, being coincident with the evaluation of the Oh model in other studies (Baghdadi and Zribi, 2011; Choker et al., 2017). The Oh model also had a large overestimation of 5.2 dB at X-band HH polarization, being much larger than those (< 1 dB) observed by Baghdadi and Zribi (2011) and Merzouki et al. (2010). The potential reason could be the calibration uncertainty of X-band data, as large offsets have been observed between different beams of the COSMO SkyMed and among different X-band missions (Pettinato et al., 2013). After removing the biases, an acceptable unbiased RMSE (ubRMSE) of < 2 dB and R of 0.4–0.8 were achieved. Therefore, correction factors were used to remove the biases as suggested by Merzouki et al. (2010), with the soil contribution in Eq. (3) for vegetated areas also being corrected.

Acceptable RMSEs (< 2.2 dB) were observed over grass and wheat paddocks for all available radar configurations except the C-band VV polarization for wheat paddocks. A large underestimation of 12.4 dB was observed for wheat at C-band VV polarization, which could be ascribed as the underestimation of transmission in the DBA (Huang et al., 2017b). More specifically, the mean field of the vegetation layer is assumed to be the incident wave on each scatterer in DBA and thus is uniform for different parts of a single cylinder (Fig. 5 a). This approximation can greatly overestimate the actual incident wave at low parts of a cylinder (Fig. 5 a) because of the increasing attenuation caused by the nearby cylinders. Consequently, the scattering field of a single cylinder was overestimated because of the overestimated incident wave, resulting in an overestimated attenuation in Eq. (3). Additionally, the assumption of equivalent medium can further underestimate the transmission of areas with a large spatial variation of vegetation density. An example is shown in Fig. 5b where the vegetation layer has an average τ_p of 4 and a 20% spatial gap without vegetation. The transmission calculated by the DBA is near 0 because of the large average τ_p; however this should be near 0.2 because of the 20% spatial gap where the signal can go through without attenuation.

The two-potential effects described by Fig. 5 tend to be more significant at C-band than L-band, with a near-zero bias for L-band at all polarizations (Zhu et al., 2019a). This can be explained by the stronger attenuation of nearby cylinders and the relatively larger gaps for a shorter wavelength. In addition, these effects relate to the geometry of the vegetation scatterers and the polarization of incident waves. In this

Table 2
Specification of SAR data in a format of incidence angle/orbit/polarization, where A and D are ascending and descending pass, respectively.

DOY	PLIS (L-band)	RADARSAT -2 (C-band)	COSMO-SkyMed (X-band)
251			33.5°/D/HH
252	20–50°/D/HH, HV, VV	39.5°/D/VV, VH	
253			28.5°/A/HH
254	20–50°/A/HH, HV, VV	22.4°/A/HH, HV, VV	
255		22.7°/D/VV, VH	
257	20–50°/D/HH, HV, VV	39.2°/A/HH, HV, VV	
260	20–50°/A/HH, HV, VV		
261			33.5°/D/HH
262	20–50°/D/HH, HV, VV	28.9°/D/VV, VH	
263			28.5°/A/HH
264		34.1°/A/VV, VH	
265	20–50°/A/HH, HV, VV		
267	20–50°/D/HH, HV, VV		
269		34.5°/D/HH, HV, VV	33.5°/D/HH
270	20–50°/A/HH, HV, VV		

study, wheat was simplified as a layer of near vertical cylinders and thus VV polarization had a more significant underestimation than HH. On the contrary, HH polarization should be more sensitive over grass as it had larger elevation angles. Fortunately, grass commonly has a relatively small VWC value of $< 1\,kg/m^2$, and only slight underestimations of 1–2 dB were observed for C- and X-band at HH polarization.

4.2. Effective radar configuration

For a given σ^0 with the knowledge of frequency, incidence angle, and polarization, the relative soil contribution (C_s) of this measurement

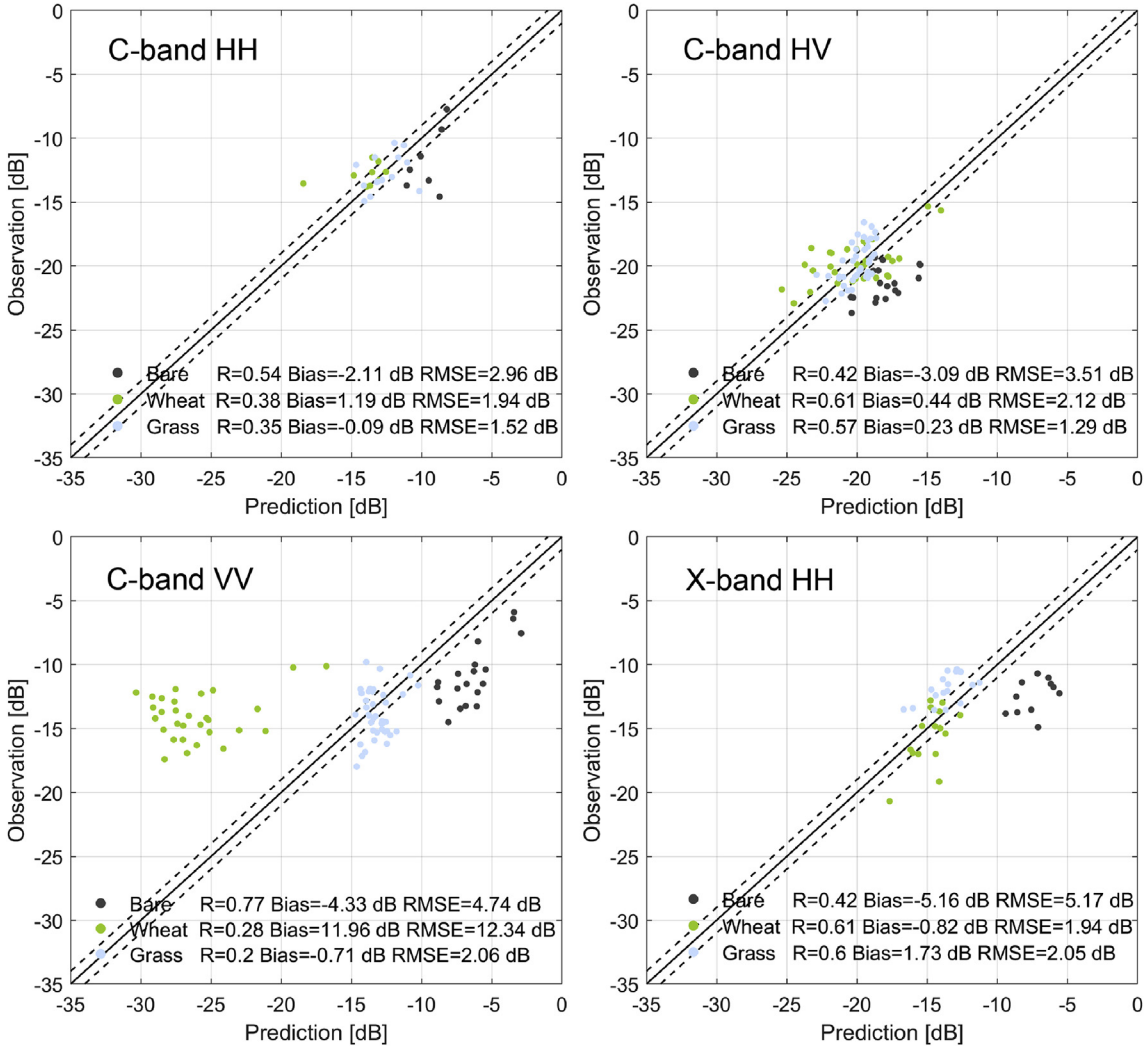

Fig. 4. Comparison of forward and observed σ^0 at the paddock scale (~ 0.1 – 0.5 km) for available C- and X-band data. The dashed lines denote the ± 1 dB offset. R refers to Pearson correlation coefficient.

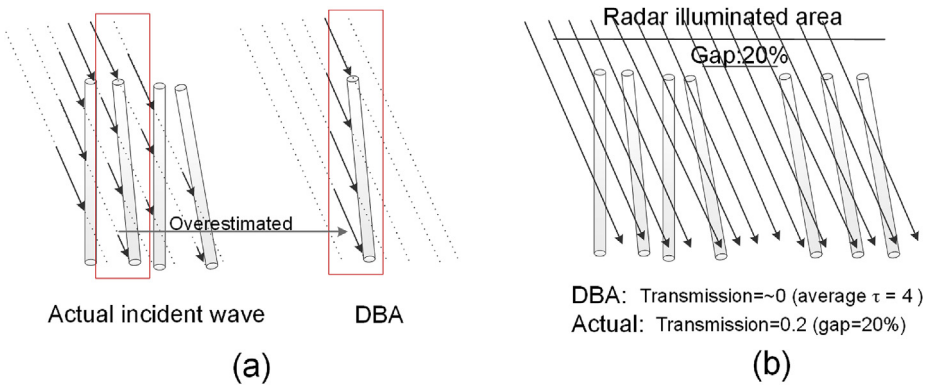

Fig. 5. Conceptual figure showing the two potential reasons for the overestimated attenuation in DBA. (a) Shows the attenuation overestimation caused by the overestimation of the incident field in a single cylinder. (b) Shows the effect of a 20% gap between vegetation stems on attenuation estimation.

and its effectiveness in soil moisture retrieval can be determined using Eq. (5). The C_s for all available data is provided in Fig. 1 (the cube named as pixel specific soil relative contribution). For the area without roughness or vegetation changes, the number of effective channels (σ^0 measurements) in soil moisture retrieval ranged from 35 – 39 out of 46 channels, with the C-band VV polarization being removed in most wheat paddocks. An investigation of the C_s for wheat is provided in Fig. 6 as an example. Not surprisingly, L-band had the largest C_s, followed by C- and X-band. Moreover, across all three frequency bands, it was observed that 1) HH polarization had the largest C_s followed by HV and VV polarization; and 2) the C_s decreased as the incidence angle and VWC increased, with the largest decrease being observed at VV polarization. An interpretation for the different response among the three polarizations is the predominant vertical structure that exists in a wheat canopy.

More specifically, a C_s of ~1 was observed for L-band at HH and HV polarization with almost no dependence on VWC and incidence angle. This can be explained by the dominant surface scattering that at HH, and the dominant double-bounce in HV with a negligible volume scattering in both polarizations. In contrast, the C_s for VV decreased to 0.5–0.9 as the VWC and incidence angle increased, because of the increased attenuation and volume scattering. The smallest C_s (~0.47) for VV was, however, still larger than the 1 dB sensitivity (0.23). This confirms the capability of L-band in soil moisture retrieval under dense wheat. C-band HH and HV polarization also showed great potential, given the considerable C_s in all cases (> 0.5). This was coincident with a number of other studies (Balenzano et al., 2011; Bousbih et al., 2017; Brown et al., 2003; Toure et al., 1994). However, C-band at VV polarization should be used carefully for wheat-like crops, because the volume scattering gradually becomes dominant as the VWC and incidence angle is increased. For a layer with a VWC of 4 kg/m^2, the C_s of C-band at VV polarization was less than 0.23 for an incidence angle larger than 27°, being 33° and 43° for a VWC of 3 kg/m^2 and 2 kg/m^2, respectively. For X-band, HH and HV polarization could still provide sufficient information about the soil surface over wheat fields, in accordance with previous experimental studies (Aubert et al., 2011; El Hajj et al., 2016). The figure also suggests a much lower validity range of VWC (< 1.5 kg/m^2) for X-band at VV polarization.

4.3. Multi-frequency retrieval

Soil moisture retrieval was made at the 25-m pixel and paddock scales respectively, using all available radar data (20 acquisitions from 15 dates). The 25 m pixel soil moisture maps for the YA7 area are depicted in Fig. 7, while the pixel and paddock scale comparison against corresponding ground measurements shown in Fig. 8. The retrieved time series soil moisture maps agree well with the dry down process observed during SMAPEx-5, with a faster dry down observed over bare soil paddocks. The observed cultivation activities in the circled paddocks were detected between DOY 267 and 269, with the sudden soil moisture increases being successfully recorded.

Moderate accuracy was achieved at the pixel scale, showing an RMSE of 0.07 – 0.08 m^3/m^3 and a correlation coefficient (R) of 0.6 – 0.8. No clear difference was found between the results of isotropic paddocks and of these with a periodic soil surface. The retrieved soil moisture for wet conditions (larger than 0.4 m^3/m^3) was slightly underestimated, which is consistent with the single L-band retrieval (Zhu et al., 2019a). Such underestimations were also observed and ascribed to the decreased sensitivity of σ^0 in moist areas in other studies (Bai et al., 2016; Wang et al., 2011). As expected, the results were greatly improved at the paddock scale. The RMSE decreased to 0.062, 0.058 and 0.054 m^3/m^3 in bare, wheat and grass, respectively, roughly reaching the 0.06 m^3/m^3 accuracy target of SMAP radar products. A good correlation (R: 0.75 – 0.87) was observed at the paddock scale with negligible biases (< 0.02 m^3/m^3). However, the retrieved accuracy was still slightly worse than the requirement of 0.05 m^3/m^3 suggested by Walker and Houser (2004) and World Meteorological Organization (http://www.wmo-sat.info/oscar/requirements).

Soil moisture retrieval was also carried out at the paddock scale using all available single- and dual-frequency series, with the results summarized in Table 3. Not surprisingly, the use of single L-band series observations retrieved better results than single C- or X-band, confirming the merit of using long wavelengths in soil moisture retrieval. The larger number of channels (polarizations) at L-band time series could be another reason for its better performance as demonstrated in Zhu et al. (2019a). Moreover, the time offset between ground measurements and the C- and X-band acquisitions could have introduced a bias of less than 0.02 m^3/m^3 in the comparison according to station measurements (Ye et al. In Review).

In contrast to expectations and earlier studies using multi-frequency data (Oh, 2004; Pierdicca et al., 2008; Zhang et al., 2016), the time series multi-frequency retrieval did not achieve the best results in this study. The L-band retrieved results were slightly deteriorated by combining the C-band series, and further deteriorated with the addition of the X-band series. Similarly, the joint use of C- and X-band series performed worse than using the C-band series alone, but better than using the X-band series alone. This could be partly explained by the relatively poor performance of using single C- and X-band series alone, which made a negative effect on the multi-frequency retrieval. Single L-band series retrieval in this study was a well-constrained inversion problem, and so additional observations (e.g., the X-band series) may only introduce noise, while those additional observations in snapshot methods (Pierdicca et al., 2008; Zhang et al., 2016) can help to turn the ill-posed L-band retrieval to a well-constrained one, thus improving the retrieval accuracy. While slight deterioration in accuracy was observed to combine C- and X-band data, the revisit was greatly enhanced to be ~1.4

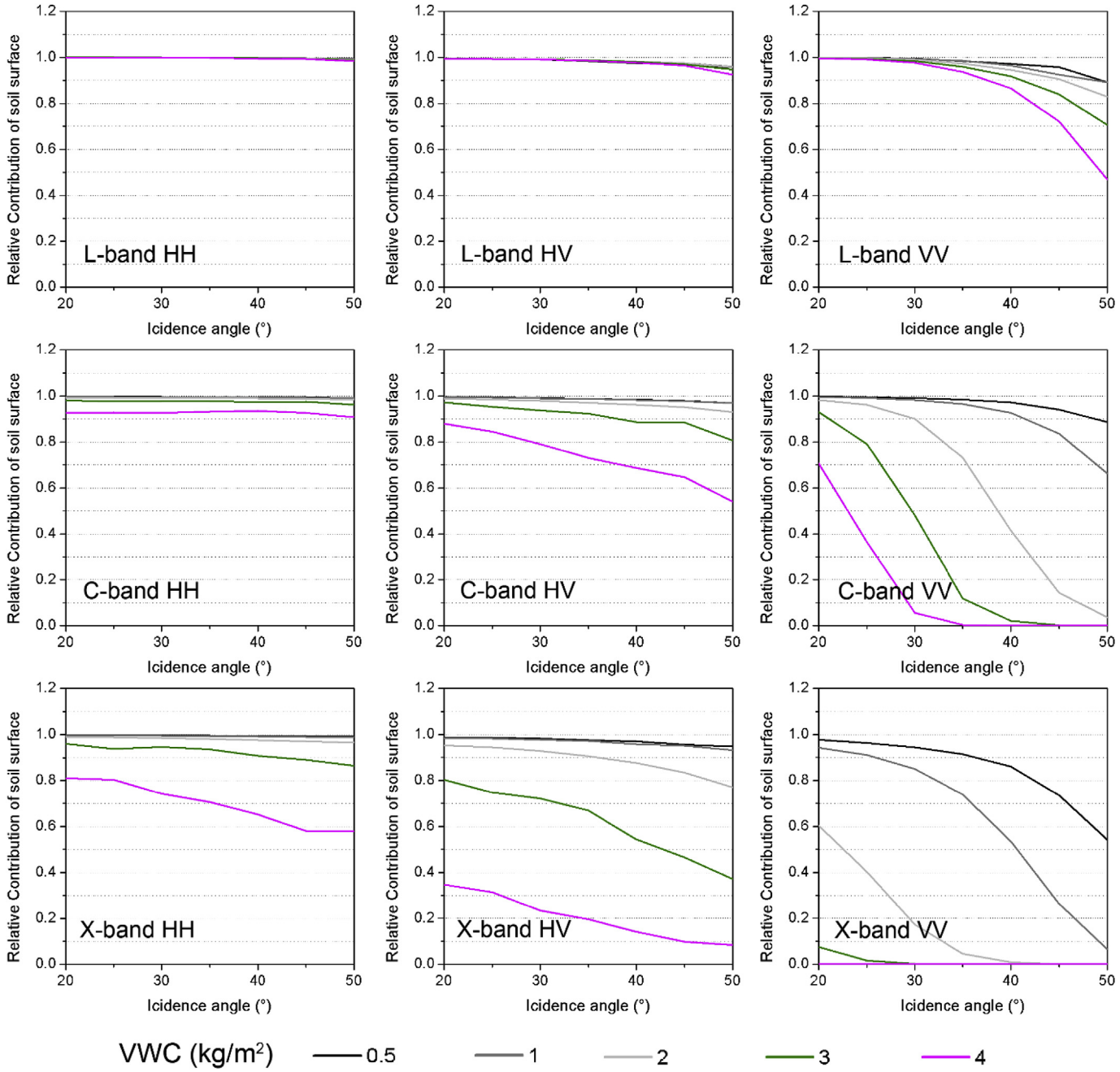

Fig. 6. Simulated relative contribution of the soil surface from under a wheat canopy. The m_v and H_R were 0.15 m^3/m^3 and 2 cm.

days during the SMAPEx-5, reaching the requirements of most applications (Engman, 1992; Walker and Houser, 2004).

The soil H_R and VWC were also retrieved using the proposed method. The results for isotropic paddocks are listed in Table 4 where only paddocks with in-situ measurements were considered. Similar to the soil moisture retrieval, the L-band observations yield the best results for H_R in single frequency retrieval, followed by C-band and X-band. Negative biases were observed at all three frequencies, with the largest bias observed at X-band, indicating that smaller effective roughness values were retrieved at shorter wavelengths. An interpretation can be the dependence of effective roughness on wavelength. Similarly, larger effective H_R were observed for long wavelengths in earlier studies calibrating the IEM (Baghdadi et al., 2004; Lievens et al., 2011). Moreover, the cost function formation used in the retrieval may also slightly change the effective roughness, with larger H_R retrieved at L-band after removing the dry-down constraint (Zhu et al., 2019a). For single frequency retrieval of VWC, C- and L-band had similar accuracy in terms of ubRMSE, while X-band achieved the best results in all four metrics; this may be explained by its larger sensitivity to vegetation. The multi-frequency retrieval of both H_R and VWC seemed to follow the same law of soil moisture retrieval, i.e., an additional frequency with poor retrieval results did not have a positive effect on the multi-frequency retrieval, suggesting that the proposed multi-frequency retrieval may not necessarily have the highest accuracy, especially when low frequency data are in abundance.

An investigation of H_R and VWC retrieval over paddocks with periodic soil surface features was also made, using the wheat paddocks with row directions nearly perpendicular or parallel to the radar look directions (Fig. 9). For those paddocks with perpendicular row features (red lines in Fig. 9), L-band had a significantly larger H_R and smaller VWC value than that retrieved from C- and X-band. This can be explained by the different effects of row structure on radar signals with

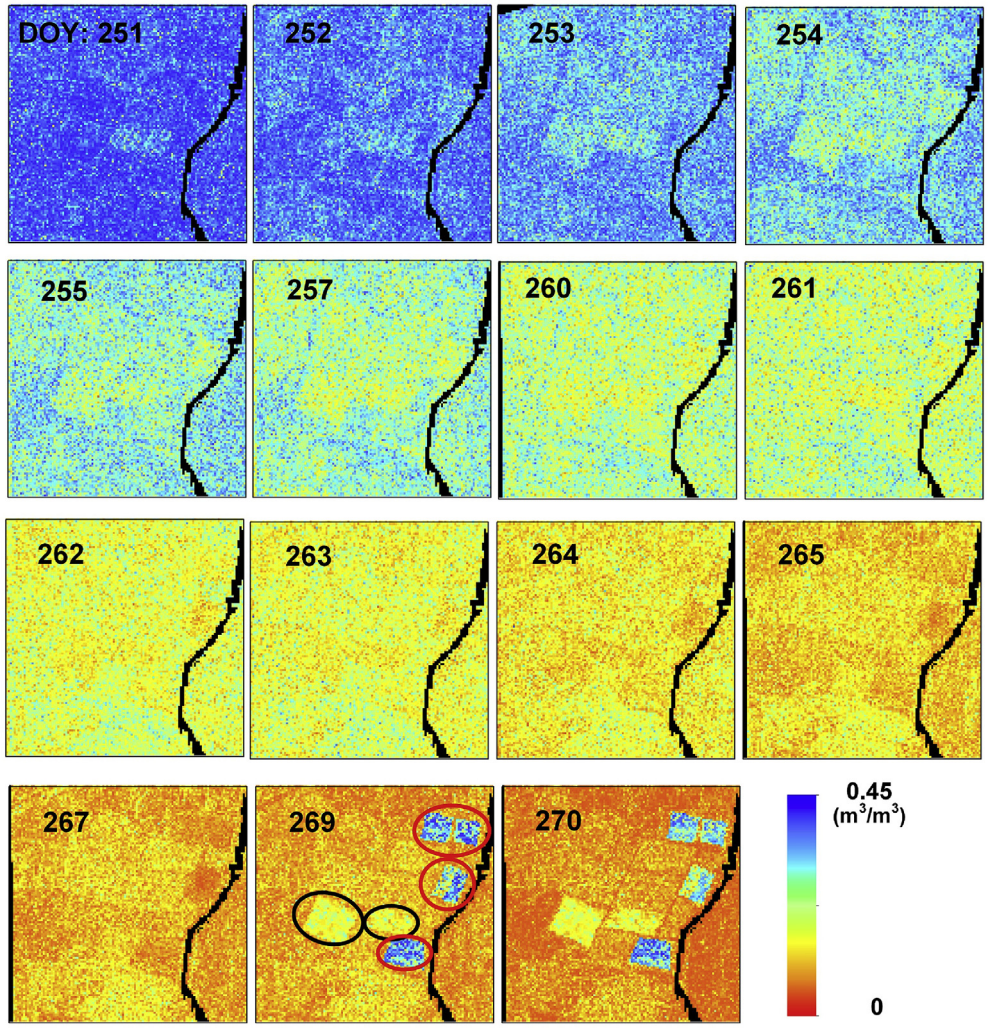

Fig. 7. Retrieved soil moisture maps in YA7 with the day of year listed in the top left. The paddocks in black circles are these with soil ploughing, while the red circles are those with irrigation. (For interpretation of the references to colour in this figure legend, the reader is referred to the Web version of this article.)

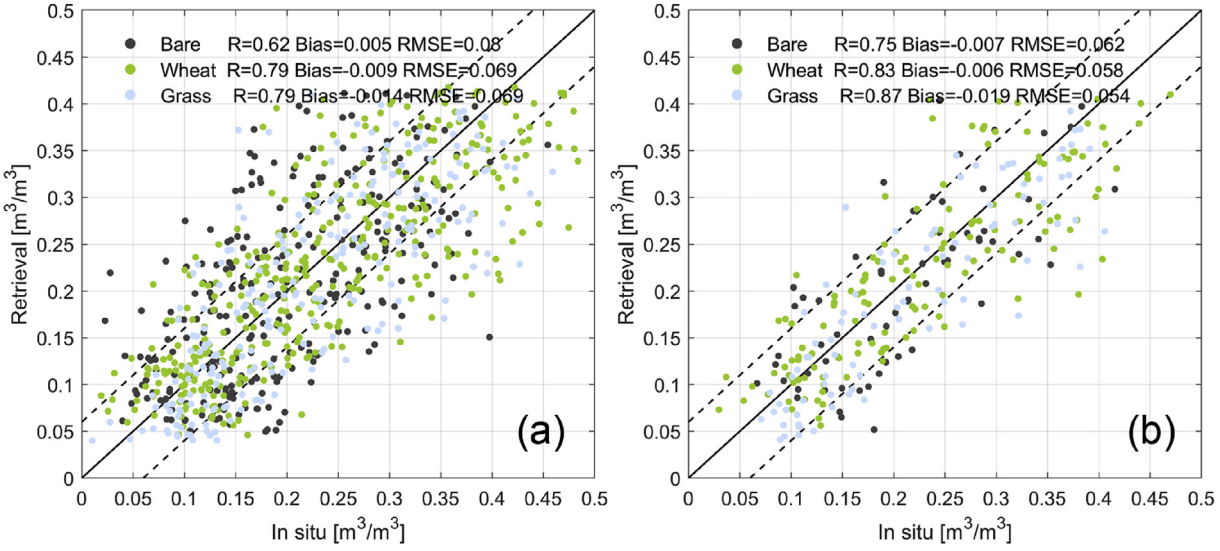

Fig. 8. In situ versus retrieved soil moisture at the 25-m pixel (a) and paddock scale (b) using time series L-, C- and X-band data. The dash lines denote the ± 0.06 m^3/m^3 target accuracy.

Table 3
Accuracy of soil moisture retrieval at the paddock scale. The bold styles denotes the best case for each land cover type.

	Bare soil			Grass			Wheat			#date/#image
	RMSE	R	Bias	RMSE	R	Bias	RMSE	R	Bias	
L[a]	**0.061**	**0.74**	**-0.012**	**0.047**	**0.91**	**-0.014**	**0.058**	**0.84**	**-0.004**	8/8
C	0.061	0.71	0.012	0.052	0.87	0.002	0.071	0.69	-0.006	7/7
X	0.080	0.50	0.021	0.065	0.80	-0.019	0.084	0.58	-0.008	5/5
L + C	0.061	0.73	-0.004	0.050	0.89	-0.022	0.059	0.82	-0.003	11/15
L + X	0.062	0.73	-0.007	0.055	0.87	0.006	0.058	0.83	0.006	13/13
C + X	0.067	0.61	-0.009	0.056	0.87	-0.026	0.071	0.80	-0.014	11/12
L + C + X	0.062	0.75	-0.007	0.054	0.87	-0.019	0.058	0.83	0.006	15/20

[a] Zhu et al. (2019a).

different wavelengths. Specifically, the co-polarized σ^0 observed perpendicular to the row structure has been found to be much larger than those observed parallelly (Blanchard and Chang, 1983; Champion and Faivre, 1996; Mattia, 2011; Ulaby and Bare, 1979; Wegmüller et al., 2011; Zribi et al., 2002). However, this effect has been found negligible for frequencies larger than 4 GHz (Ulaby and Bare, 1979). Consequently, for perpendicular rows, larger H_R and smaller VWC values were retrieved at longer wavelengths in order to have a larger soil surface scattering and a smaller vegetation attenuation. For paddocks with parallel row features (black lines in Fig. 9), L-band tended to have similar H_R and VWC with C- and X-band, confirming the reduced effect of parallel row structures.

With respect to multi-frequency retrieval, the combinations of L + C, L + X, and L + C + X retrieved a similar H_R compared to that of the single L-band retrieval, especially for those with perpendicular row structures. The potential reason is that L-band is more sensitive to the row structure and thus was dominant in the cost function. Multi-frequency VWC retrieval seemed to have a value similar to the average of the values retrieved by single frequency series. For instance, the combination of L + X series had a VWC of 1.4 kg/m^2 in paddocks #80, #98 and #115, which was close to the average value from X-band (2.3 kg/m^2) and L-band (0.84 kg/m^2) retrievals on their own. This may suggest that multi-frequency retrievals may not necessarily have the best results but can be less sensitive to effect of complex surface conditions, e.g., the effect of periodic features at long wavelengths. Moreover, this also confirms the risk of sharing retrieved VWC and H_R among different radar configurations.

4.4. The effect of abrupt cultivation activities

The performance of the whole framework was presented in previous sections. Here, the effect of the change detection information produced by the first step on soil moisture retrieval was investigated, using a comparison with soil moisture retrieval without change detection information. The results of six selected paddocks with cultivation activities is shown in Fig. 10. Other paddocks with cultivation activities were not included because of the similar results. For example, the proposed method had similar results over paddock #48 and #30 as depicted in the time series soil moisture maps (Fig. 7) and thus only paddock #48 was included for discussion.

In general, the dry down process was successfully captured by both approaches (with/without change detection) with the main differences after the roughness changes or irrigation. The soil moisture retrieved with the change detection information showed a sudden increase after both soil tillage and irrigation in all paddocks, which is consistent with the ground observations in paddocks #54, #103, #110 and #113. Since the shadow root zone commonly has higher soil moisture than the surface layer (< 5 cm), a slight increase of soil moisture after the soil practice was also expected for paddocks #2 and #48. This suggests that the proposed method can accurately reflect the soil moisture evolution in time despite the split of time series in the presence of cultivations activities. In view of RMSE, the integration of change detection information outperformed in five of six cases, especially for these with irrigation events. Different from other multi-temporal methods, an additional dry down constraint was used here. The preprocessing step of change detection potentially ensure both the dry down constraint and the assumption of time-invariant roughness and VWC is met.

5. Conclusion and discussions

A multi-frequency soil moisture retrieval framework was presented to be compatible with SAR missions operating at the commonly used remote sensing frequency bands, i.e., L-, C- and X-band. Development of the proposed framework starts from solving an ill-posed problem and takes all the available data as equally weighted input. This choice, however, has not fully utilized the merit of multi-frequency data which responds differently to surface biophysical parameters. For instance, the X-band observations contain valuable information of vegetation (Solberg et al., 2010; Wallington and Woodhouse, 2006) and thus VWC derived from single C- or X-band data may be used in the soil moisture retrieval from other frequency bands. However, the uncertainty of such a step may deteriorate the subsequent soil moisture retrieval despite the complex VWC retrieval process. Fig. 9 and many earlier studies have confirmed the risk to reuse roughness parameters among different radar configurations (Baghdadi et al., 2004; Lievens et al., 2011; Zhu et al., 2016).

Table 4
Accuracy of H_R and VWC retrieval at the paddock scale. The bold styles denote the best case in RMSE. The ubRMSE refers to the unbiased RMSE.

	H_R (cm)				VWC (kg/m^2)			
	RMSE	R	Bias	ubRMSE	RMSE	R	Bias	ubRMSE
L	**0.397**	**0.577**	**-0.084**	**0.389**	0.775	0.506	0.054	0.773
C	0.664	0.034	-0.509	0.426	1.008	0.603	0.449	0.802
X	1.080	0.002	-0.693	0.828	**0.590**	**0.651**	**-0.063**	**0.587**
L + C	0.469	0.361	-0.145	0.447	0.799	0.713	0.310	0.737
L + X	0.428	0.425	-0.122	0.411	0.610	0.695	-0.039	0.609
C + X	1.069	-0.041	-0.680	0.851	0.695	0.697	0.145	0.680
L + C + X	0.406	0.551	-0.121	0.356	0.646	0.708	0.191	0.617

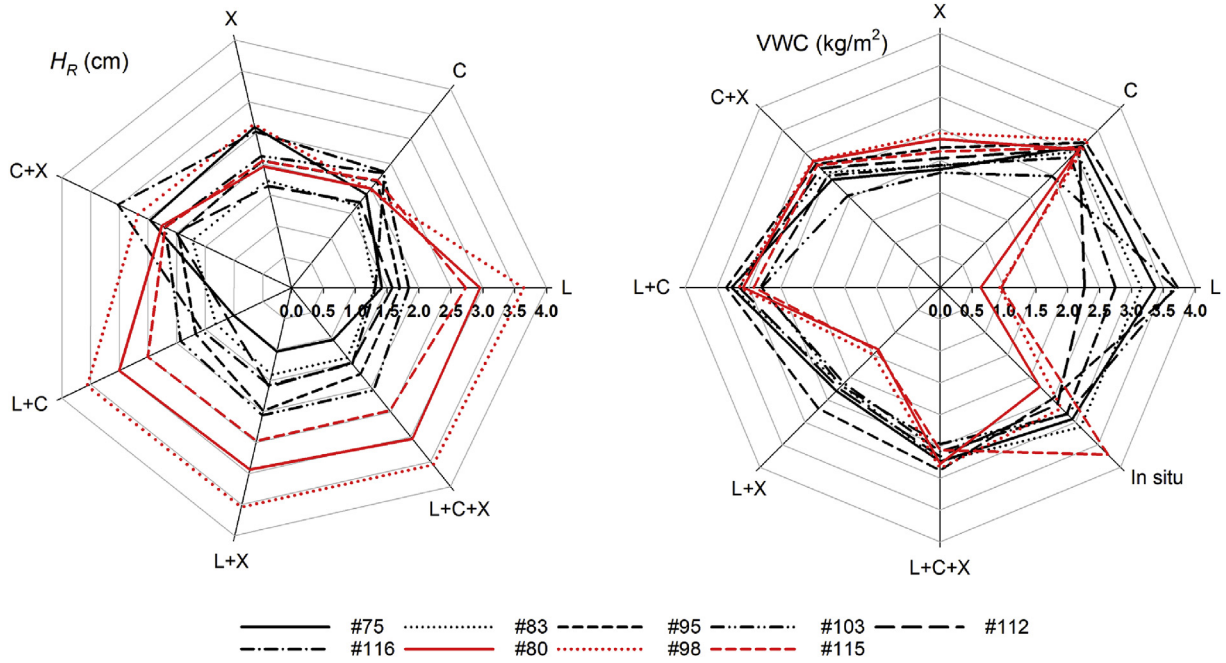

Fig. 9. Retrieved effective H_R and VWC values for wheat paddocks with a periodical soil surface. The red and black lines are paddocks with a row direction perpendicular and parallel to the radar look direction, respectively. (For interpretation of the references to colour in this figure legend, the reader is referred to the Web version of this article.)

More observations also mean more unknowns to be determined, as the perceived soil moisture and roughness are different among different radar systems (Ulaby et al., 2014). Configuration specific calibration is thus required with more empirical parameters to be determined, e.g., the calibration in (Baghdadi et al., 2004; Hosseini and McNairn, 2017). In contrast, several assumptions were made in the proposed method to reduce the number of unknowns. A homogeneous soil moisture profile was assumed for the soil layer above the penetration depth of L-band (~ 5 cm) and thus L-, C- and X-band have the same apparent soil moisture in the proposed multi-frequency retrieval. This assumption, however, can introduce large uncertainty in semiarid and arid areas with heterogeneous vertical profiles (Amri et al., 2012; Le Morvan et al., 2008; Ulaby et al., 1996). Moreover, Zribi et al. (2014b) have shown that the consideration of soil moisture vertical variation can substantially

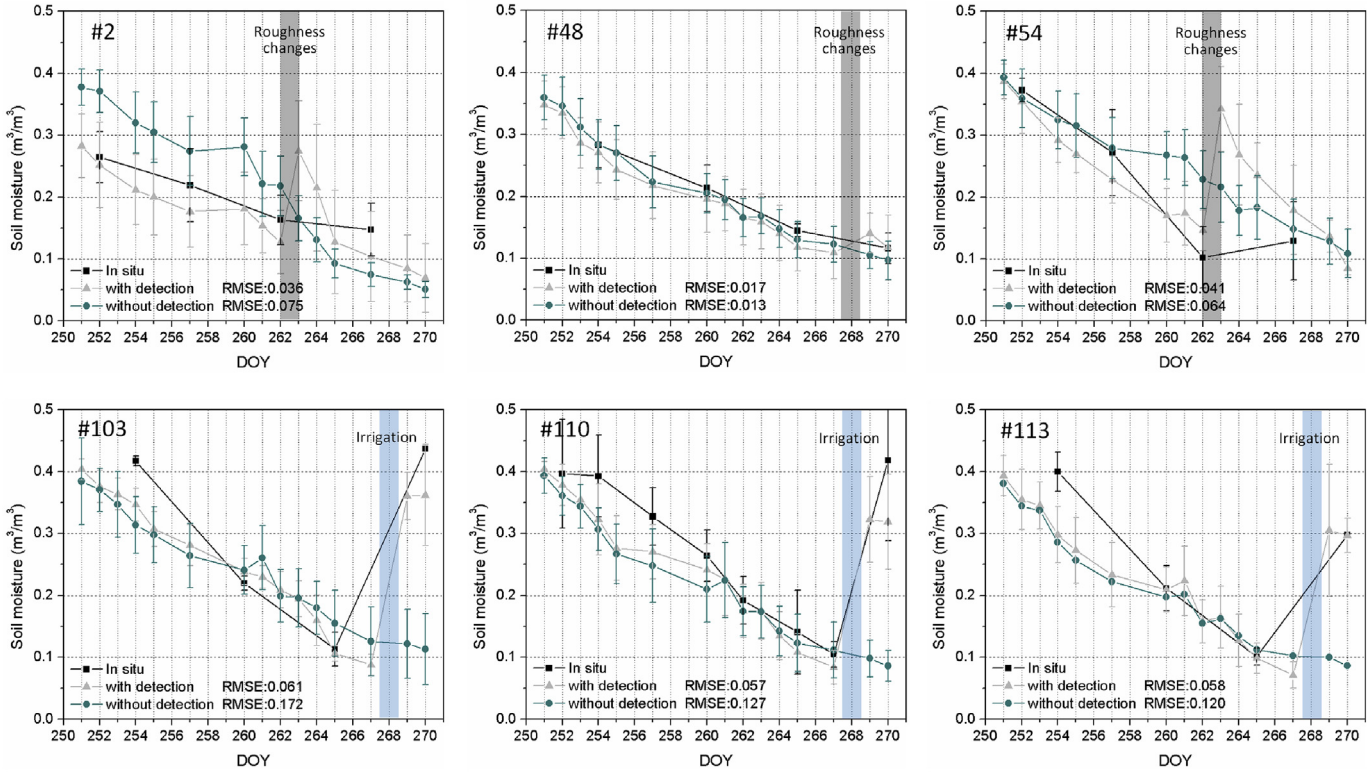

Fig. 10. Time series average soil moisture of paddocks with/without integrating change detection results. The error bar denotes the standard deviation.

improve the soil surface scattering prediction at C- and X-band. Time-invariant physical roughness and vegetation was assumed to eliminate the effect of natural roughness and vegetation evolution, with an effective isotropic H_R being assumed to represent the perceived roughness of the available radar configurations at each retrieval grid. Different effective roughness values were achieved for single-, dual- and triple-frequency retrieval (Fig. 9) as expected, further confirming the risk of parameters sharing among multi-frequency retrieval.

To ensure the two key assumptions were complied with, two pre-processing steps were integrated into the proposed framework. The effectiveness of change detection was confirmed, showing a significant improvement of up to 0.1 m^3/m^3 for areas with cultivation activities. As for the step to determine the effectiveness of a radar input, sensitive analysis has been widely used in soil moisture retrieval (Bousbih et al., 2017; Kim and Van Zyl, 2009; Quesney et al., 2000; Zribi et al., 2007). The main advantage of the proposed method is its independence from scenario-specific sensitivity analysis and the nature of model-oriented, with the disadvantage being the need for complex vegetation scattering modeling. Specifically, the effectiveness of the radar configurations presented in Section 4.2 were determined in view of the forward models used in soil moisture retrieval, rather than being an assessment of the real capability of radar systems. For example, the C-band VV had a significantly overestimated attenuation in DBA, thus being noise in the subsequent DBA-based soil moisture retrieval. However, this conclusion may be not true for real SAR systems and/or other studies using different models (e.g., a calibrated water cloud model), but is suitable for this study because the DBA was used for soil moisture retrieval. This also suggests that the direct use of model-based conclusions in other studies can be questionable.

Evaluation based on the SMAPEx-5 dataset consisting of L-band airborne data, C-band RADARSAT-2 data and X-band COSMO-SkyMed data confirmed the robustness of the proposed framework, showing an acceptable overall RMSE of 0.058 cm^3/cm^3 at the paddock scale (~0.1 – 0.5 km). The DBA was confirmed to underestimate the VV polarization at C-band. The comparison with single and dual frequency retrieval suggests that multi-frequency retrieval does not necessarily provide the highest accuracy. However, it is still valuable to joint use multi-frequency data consider the limited deterioration in accuracy and significantly enhanced temporal resolution for capture the soil moisture variation over time. The proposed framework is compatible with the C-band Sentinel-1 and L-band SAOCOM constellation, providing a promising alternative for global soil moisture mapping with an adequate spatial (< 100 m) and temporal (< 3 days) resolution. Future works for large scale application include i) the development of LUTs for other vegetation types and ii) comprehensive evaluation of the assumptions and simplifications discussed above. Moreover, an effective way to use the multi-frequency data in a complementary manner is suggested for improved soil moisture retrieval.

Acknowledgements

The SMAPEx-5 field campaigns were supported by an Australian Research Council Discovery Project (DP1401-00572). The authors wish to thank all the SMAPEx-5 experiment participants. The authors also acknowledge the scholarships awarded by China Scholarship Council (CSC) and Monash University to support Liujun Zhu's PhD research and visiting in the University of Michigan, USA.

References

Altese, E., Bolognani, O., Mancini, M., Troch, P.A., 1996. Retrieving soil moisture over bare soil from ERS 1 synthetic aperture radar data: sensitivity analysis based on a theoretical surface scattering model and field data. Water Resour. Res. 32, 653–661.
Amri, R., Zribi, M., Lili-Chabaane, Z., Wagner, W., Hasenauer, S., 2012. Analysis of C-band scatterometer moisture estimations derived over a semiarid region. IEEE Trans. Geosci. Remote Sens. 50, 2630–2638.
Attema, E., Ulaby, F.T., 1978. Vegetation modeled as a water cloud. Radio Sci. 13, 357–364.
Aubert, M., Baghdadi, N., Zribi, M., Douaoui, A., Loumagne, C., Baup, F., El Hajj, M., Garrigues, S., 2011. Analysis of TerraSAR-X data sensitivity to bare soil moisture, roughness, composition and soil crust. Remote Sens. Environ. 115, 1801–1810.
Baghdadi, N., Choker, M., Zribi, M., Hajj, M., Paloscia, S., Verhoest, N., Lievens, H., Baup, F., Mattia, F., 2016. A new empirical model for radar scattering from bare soil surfaces. Remote Sens. 8, 920.
Baghdadi, N., Gherboudj, I., Zribi, M., Sahebi, M., King, C., Bonn, F., 2004. Semi-empirical calibration of the IEM backscattering model using radar images and moisture and roughness field measurements. Int. J. Remote Sens. 25, 3593–3623.
Baghdadi, N., Zribi, M., 2006. Evaluation of radar backscatter models IEM, OH and Dubois using experimental observations. Int. J. Remote Sens. 27, 3831–3852.
Baghdadi, N., Zribi, M., 2011. Evaluation of radar backscatter models IEM, OH and Dubois using experimental observations. Int. J. Remote Sens. 27, 3831–3852.
Bai, X., He, B., Li, X., 2016. Optimum surface roughness to parameterize advanced integral equation model for soil moisture retrieval in prairie area using Radarsat-2 data. IEEE Trans. Geosci. Remote Sens. 54, 2437–2449.
Bai, X., He, B., Xing, M., Li, X., 2015. Method for soil moisture retrieval in arid prairie using TerraSAR-X data. J. Appl. Remote Sens. 9 096062-096062.
Balenzano, A., Mattia, F., Satalino, G., Davidson, M.W., 2011. Dense temporal series of C- and L-band SAR data for soil moisture retrieval over agricultural crops. Ieee Journal of Selected Topics in Applied Earth Observations and Remote Sensing 4, 439–450.
Bindlish, R., Barros, A.P., 2000. Multifrequency soil moisture inversion from SAR measurements with the use of IEM. Remote Sens. Environ. 71, 67–88.
Bindlish, R., Barros, A.P., 2001. Parameterization of vegetation backscatter in radar-based, soil moisture estimation. Remote Sens. Environ. 76, 130–137.
Blanchard, B., Chang, A., 1983. Estimation of soil moisture from Seasat SAR data. J. Am. Water Resour. Assoc. 19, 803–810.
Bousbih, S., Zribi, M., Lili-Chabaane, Z., Baghdadi, N., El Hajj, M., Gao, Q., Mougenot, B., 2017. Potential of sentinel-1 radar data for the assessment of soil and cereal cover parameters. Sensors 17, 2617.
Brown, S.C., Quegan, S., Morrison, K., Bennett, J.C., Cookmartin, G., 2003. High-resolution measurements of scattering in wheat canopies-Implications for crop parameter retrieval. IEEE Trans. Geosci. Remote Sens. 41, 1602–1610.
Champion, I., Faivre, R., 1996. The field row direction relative to the radar azimuth considered as an apparent surface roughness for smooth bare soils. Int. J. Remote Sens. 17, 3305–3311.
Choker, M., Baghdadi, N., Zribi, M., El Hajj, M., Paloscia, S., Verhoest, N.E., Lievens, H., Mattia, F., 2017. Evaluation of the Oh, Dubois and IEM backscatter models using a large dataset of SAR data and experimental soil measurements. Water 9, 38.
Christensen, E.L., Skou, N., Dall, J., Woelders, K.W., Jorgensen, J.H., Granholm, J., Madsen, S.N., 1998. EMISAR: an absolutely calibrated polarimetric L-and C-band SAR. IEEE Trans. Geosci. Remote Sens. 36, 1852–1865.
Dobson, M.C., Ulaby, F.T., Hallikainen, M.T., El-Rayes, M., 1985. Microwave dielectric behavior of wet soil-Part II: dielectric mixing models. Geoscience and Remote Sensing, IEEE Transactions on 35–46.
Dubois, P.C., Van Zyl, J., Engman, T., 1995. Measuring soil moisture with imaging radars. IEEE Trans. Geosci. Remote Sens. 33, 915–926.
El Hajj, M., Baghdadi, N., Bazzi, H., Zribi, M., 2019. Penetration analysis of SAR signals in the C and L bands for wheat, maize, and grasslands. Remote Sens. 11, 31.
El Hajj, M., Baghdadi, N., Zribi, M., Belaud, G., Cheviron, B., Courault, D., Charron, F., 2016. Soil moisture retrieval over irrigated grassland using X-band SAR data. Remote Sens. Environ. 176, 202–218.
Engman, E.T., 1992. Soil moisture needs in earth sciences. 1992 IEEE International Geoscience and Remoe Sensing Symposium (IGARSS) 1, 477–479.
Fung, A.K., 1994. Microwave Scattering and Emission Models and Their Applications. Artech House.
Hosseini, M., McNairn, H., 2017. Using multi-polarization C-and L-band synthetic aperture radar to estimate biomass and soil moisture of wheat fields. Int. J. Appl. Earth Obs. Geoinf. 58, 50–64.
Huang, H., Liao, T.-H., Tsang, L., Njoku, E.G., Colliander, A., Jackson, T.J., Burgin, M.S., Yueh, S., 2017a. Modelling and validation of combined active and passive microwave remote sensing of agricultural vegetation at L-band. Progress In Electromagnetics Research 78, 91–124.
Huang, H., Tsang, L., Njoku, E.G., Colliander, A., Liao, T.-H., Ding, K.-H., 2017b. Propagation and scattering by a layer of randomly distributed dielectric cylinders using Monte Carlo simulations of 3D Maxwell equations with applications in microwave interactions with vegetation. IEEE Access 5, 11985–12003.
Huang, S., Tsang, L., 2012. Electromagnetic scattering of randomly rough soil surfaces based on numerical solutions of Maxwell equations in three-dimensional simulations using a hybrid UV/PBTG/SMCG method. IEEE Trans. Geosci. Remote Sens. 50, 4025–4035.
Huang, S., Tsang, L., Njoku, E.G., Chan, K.S., 2010. Backscattering coefficients, coherent reflectivities, and emissivities of randomly rough soil surfaces at L-band for SMAP applications based on numerical solutions of Maxwell equations in three-dimensional simulations. IEEE Trans. Geosci. Remote Sens. 48, 2557–2568.
Huang, Y., Walker, J.P., Gao, Y., Wu, X., Monerris, A., 2016. Estimation of vegetation water content from the radar vegetation index at L-band. IEEE Trans. Geosci. Remote Sens. 54, 981–989.
Jackson, T., Bras, R., England, A., 1999. Soil moisture research mission (EX-4). In: NASA Post-2002 Land Surface Hydrology Mission Workshop. NASA, Irvine, CA.
Jackson, T., McNairn, H., Weltz, M., Brisco, B., Brown, R., 1997. First order surface roughness correction of active microwave observations for estimating soil moisture. IEEE Trans. Geosci. Remote Sens. 35, 1065–1069.
Joseph, A., van der Velde, R., O'Neill, P., Lang, R., Gish, T., 2010. Effects of corn on C-and L-band radar backscatter: a correction method for soil moisture retrieval. Remote

Sens. Environ. 114, 2417–2430.
Joseph, A.T., van der Velde, R., O'Neill, P.E., Lang, R.H., Gish, T., 2008. Soil moisture retrieval during a corn growth cycle using L-band (1.6 GHz) radar observations. IEEE Trans. Geosci. Remote Sens. 46, 2365–2374.
Kim, S.-b., Arii, M., Jackson, T., 2017. Modeling L-band synthetic aperture radar data through dielectric changes in soil moisture and vegetation over shrublands. Ieee Journal of Selected Topics in Applied Earth Observations and Remote Sensing 10, 4753–4762.
Kim, S.-B., Moghaddam, M., Tsang, L., Burgin, M., Xu, X., Njoku, E.G., 2014a. Models of L-band radar backscattering coefficients over global terrain for soil moisture retrieval. IEEE Trans. Geosci. Remote Sens. 52, 1381–1396.
Kim, S.-B., Tsang, L., Johnson, J.T., Huang, S., Van Zyl, J.J., Njoku, E.G., 2012a. Soil moisture retrieval using time-series radar observations over bare surfaces. IEEE Trans. Geosci. Remote Sens. 50, 1853–1863.
Kim, Y., Jackson, T., Bindlish, R., Hong, S., Jung, G., Lee, K., 2014b. Retrieval of wheat growth parameters with radar vegetation indices. Parameters 20, 23.
Kim, Y., Jackson, T., Bindlish, R., Lee, H., Hong, S., 2012b. Radar vegetation index for estimating the vegetation water content of rice and soybean. IEEE Geosci. Remote Sens. Lett. 9, 564–568.
Kim, Y., Van Zyl, J.J., 2009. A time-series approach to estimate soil moisture using polarimetric radar data. IEEE Trans. Geosci. Remote Sens. 47, 2519–2527.
Kornelsen, K.C., Coulibaly, P., 2013. Advances in soil moisture retrieval from synthetic aperture radar and hydrological applications. J. Hydrol. 476, 460–489.
Kweon, S.-K., Oh, Y., 2014. Estimation of soil moisture and surface roughness from single-polarized radar data for bare soil surface and comparison with dual-and quad-polarization cases. IEEE Trans. Geosci. Remote Sens. 52, 4056–4064.
Lang, R.H., Sighu, J.S., 1983. Electromagnetic backscattering from a layer of vegetation: a discrete approach. IEEE Trans. Geosci. Remote Sens. 62–71.
Le Morvan, A., Zribi, M., Baghdadi, N., Chanzy, A., 2008. Soil moisture profile effect on radar signal measurement. Sensors 8, 256–270.
Liao, T.-H., Tsang, L., Huang, S., Niamsuwan, N., Jaruwatanadilok, S., Kim, S.-b., Ren, H., Chen, K.-L., 2016. Copolarized and cross-polarized backscattering from random rough soil surfaces from L-Band to Ku-Band using numerical solutions of Maxwell's equations with near-field precondition. IEEE Trans. Geosci. Remote Sens. 54, 651–662.
Lievens, H., Verhoest, N.E., Keyser, E.D., Vernieuwe, H., Matgen, P., Álvarez-Mozos, J., Baets, B.D., 2011. Effective roughness modelling as a tool for soil moisture retrieval from C-and L-band SAR. Hydrol. Earth Syst. Sci. 15, 151–162.
Mancini, M., Hoeben, R., Troch, P.A., 1999. Multifrequency radar observations of bare surface soil moisture content: a laboratory experiment. Water Resour. Res. 35, 1827–1838.
Mattia, F., 2011. Coherent and incoherent scattering from tilled soil surfaces. Waves Random Complex Media 21, 278–300.
Mattia, F., Satalino, G., Pauwels, V., Loew, A., 2009. Soil moisture retrieval through a merging of multi-temporal L-band SAR data and hydrologic modelling. Hydrol. Earth Syst. Sci. 13, 343–356.
McNairn, H., Merzouki, A., Pacheco, A., Fitzmaurice, J., 2012. Monitoring soil moisture to support risk reduction for the agriculture sector using RADARSAT-2. IEEE Journal ofSelected Topics in Applied Earth Observations and Remote Sensing 5, 824–834.
Merlin, O., Walker, J., Panciera, R., Young, R., Kalma, J., Kim, E., 2007. Calibration of a soil moisture sensor in heterogeneous terrain. In: Oxley, L., Kulasiri, D. (Eds.), 2007 International Congress on Modelling and Simulation (MODSIM), pp. 2604–2610 (Modelling and Simulation Society of Australia and New Zealand).
Merzouki, A., McNairn, H., Pacheco, A., 2010. Evaluation of the Dubois, Oh, and IEM radar backscatter models over agricultural fields using C-band RADARSAT-2 SAR image data. Can. J. Remote Sens. 36, S274–S286.
Mirsoleimani, H.R., Sahebi, M.R., Baghdadi, N., El Hajj, M., 2019. Bare soil surface moisture retrieval from sentinel-1 SAR data based on the calibrated IEM and dubois models using neural networks. Sensors 19, 3209.
Moghaddam, M., Saatchi, S., 1995. Analysis of scattering mechanisms in SAR imagery over boreal forest: results from BOREAS'93. IEEE Trans. Geosci. Remote Sens. 33, 1290–1296.
Moghaddam, M., Saatchi, S., Cuenca, R.H., 2000. Estimating subcanopy soil moisture with radar. J. Geophys. Res.: Atmosphere 105, 14899–14911.
Notarnicola, C., 2014. A bayesian change detection approach for retrieval of soil moisture variations under different roughness conditions. IEEE Geosci. Remote Sens. Lett. 11, 414–418.
Notarnicola, C., Angiulli, M., Posa, F., 2008. Soil moisture retrieval from remotely sensed data: neural network approach versus Bayesian method. IEEE Trans. Geosci. Remote Sens. 46, 547–557.
Oh, Y., 2004. Quantitative retrieval of soil moisture content and surface roughness from multipolarized radar observations of bare soil surfaces. IEEE Trans. Geosci. Remote Sens. 42, 596–601.
Oh, Y., Sarabandi, K., Ulaby, F.T., 1992. An empirical model and an inversion technique for radar scattering from bare soil surfaces. IEEE Trans. Geosci. Remote Sens. 30, 370–381.
Oh, Y., Sarabandi, K., Ulaby, F.T., 2002. Semi-empirical model of the ensemble-averaged differential Mueller matrix for microwave backscattering from bare soil surfaces. IEEE Trans. Geosci. Remote Sens. 40, 1348–1355.
Ouellette, J.D., Johnson, J.T., Balenzano, A., Mattia, F., Satalino, G., Kim, S.-B., Dunbar, R.S., Colliander, A., Cosh, M.H., Caldwell, T.G., 2017. A time-series approach to estimating soil moisture from vegetated surfaces using L-band radar backscatter. IEEE Trans. Geosci. Remote Sens. 55, 3186–3193.
Paloscia, S., Pampaloni, P., Pettinato, S., Santi, E., 2008. A comparison of algorithms for retrieving soil moisture from ENVISAT/ASAR images. IEEE Trans. Geosci. Remote Sens. 46, 3274–3284.
Panciera, R., Tanase, M.A., Lowell, K., Walker, J.P., 2014. Evaluation of IEM, Dubois, and Oh radar backscatter models using airborne L-band SAR. IEEE Trans. Geosci. Remote Sens. 52, 4966–4979.
Pasolli, L., Notarnicola, C., Bertoldi, G., Bruzzone, L., Remelgado, R., Greifeneder, F., Niedrist, G., Della Chiesa, S., Tappeiner, U., Zebisch, M., 2015. Estimation of soil moisture in mountain areas using SVR technique applied to multiscale Active radar images at C-band. Ieee Journal of Selected Topics in Applied Earth Observations and Remote Sensing 8, 262–283.
Pettinato, S., Santi, E., Paloscia, S., Pampaloni, P., Fontanelli, G., 2013. The intercomparison of X-band SAR images from COSMO-SkyMed and TerraSAR-X satellites: case studies. Remote Sens. 5, 2928–2942.
Pierdicca, N., Castracane, P., Pulvirenti, L., 2008. Inversion of electromagnetic models for bare soil parameter estimation from multifrequency polarimetric SAR data. Sensors 8, 8181–8200.
Pierdicca, N., Pulvirenti, L., Bignami, C., 2010. Soil moisture estimation over vegetated terrains using multitemporal remote sensing data. Remote Sens. Environ. 114, 440–448.
Quesney, A., Le Hégarat-Mascle, S., Taconet, O., Vidal-Madjar, D., Wigneron, J., Loumagne, C., Normand, M., 2000. Estimation of watershed soil moisture index from ERS/SAR data. Remote Sens. Environ. 72, 290–303.
Rahman, M., Moran, M., Thoma, D., Bryant, R., Collins, C.H., Jackson, T., Orr, B., Tischler, M., 2008. Mapping surface roughness and soil moisture using multi-angle radar imagery without ancillary data. Remote Sens. Environ. 112, 391–402.
Satalino, G., Mattia, F., Davidson, M.W., Le Toan, T., Pasquariello, G., Borgeaud, M., 2002. On current limits of soil moisture retrieval from ERS-SAR data. IEEE Trans. Geosci. Remote Sens. 40, 2438–2447.
Shen, X., Mao, K., Qin, Q., Hong, Y., Zhang, G., 2013. Bare surface soil moisture estimation using double-angle and dual-polarization L-band radar data. IEEE Trans. Geosci. Remote Sens. 51, 3931–3942.
Shi, J., Wang, J., Hsu, A.Y., O'Neill, P.E., Engman, E.T., 1997. Estimation of bare surface soil moisture and surface roughness parameter using L-band SAR image data. IEEE Trans. Geosci. Remote Sens. 35, 1254–1266.
Shimada, M., Isoguchi, O., Tadono, T., Isono, K., 2009. PALSAR radiometric and geometric calibration. IEEE Trans. Geosci. Remote Sens. 47, 3915–3932.
Solberg, S., Astrup, R., Gobakken, T., Næsset, E., Weydahl, D.J., 2010. Estimating spruce and pine biomass with interferometric X-band SAR. Remote Sens. Environ. 114, 2353–2360.
Srivastava, H.S., Patel, P., Sharma, Y., Navalgund, R.R., 2009. Large-area soil moisture estimation using multi-incidence-angle RADARSAT-1 SAR data. IEEE Trans. Geosci. Remote Sens. 47, 2528–2535.
Toure, A., Thomson, K.P., Edwards, G., Brown, R.J., Brisco, B.G., 1994. Adaptation of the MIMICS backscattering model to the agricultural context-wheat and canola at L and C bands. IEEE Trans. Geosci. Remote Sens. 32, 47–61.
Tsang, L., Liao, T.-H., Tan, S., Huang, H., Qiao, T., 2017. Microwave remote sensing of soil, ocean, snow and vegetation based on 3D Numerical Solutions of Maxwell Equations (NMM3D). In: 2017 IEEE International Geoscience and Remote Sensing Symposium (IGARSS). IEEE, pp. 1413–1414.
Ulaby, F.T., Bare, J., 1979. Look direction modulation function of the radar backscattering coeffieient of agricultural fields. Photogramm. Eng. Remote Sens. 45 (11), 1495–1506.
Ulaby, F.T., Dubois, P.C., Van Zyl, J., 1996. Radar mapping of surface soil moisture. J. Hydrol. 184, 57–84.
Ulaby, F.T., Long, D.G., Blackwell, W.J., Elachi, C., Fung, A.K., Ruf, C., Sarabandi, K., Zebker, H.A., Van Zyl, J., 2014. Microwave Radar and Radiometric Remote Sensing. The University of Michigan Press, Ann Arbor.
Ulaby, F.T., Sarabandi, K., Mcdonald, K., Whitt, M., Dobson, M.C., 1990. Michigan microwave canopy scattering model. Int. J. Remote Sens. 11, 1223–1253.
van der Velde, R., Su, Z., van Oevelen, P., Wen, J., Ma, Y., Salama, M.S., 2012. Soil moisture mapping over the central part of the Tibetan Plateau using a series of ASAR WS images. Remote Sens. Environ. 120, 175–187.
Wagner, W., Lemoine, G., Rott, H., 1999. A method for estimating soil moisture from ERS scatterometer and soil data. Remote Sens. Environ. 70, 191–207.
Walker, J.P., Houser, P.R., 2004. Requirements of a global near-surface soil moisture satellite mission: accuracy, repeat time, and spatial resolution. Adv. Water Resour. 27, 785–801.
Wallington, E.D., Woodhouse, I.H., 2006. Forest height retrieval from commercial X-band SAR products. IEEE Trans. Geosci. Remote Sens. 44, 863–870.
Wang, S., Li, X., Han, X., Jin, R., 2011. Estimation of surface soil moisture and roughness from multi-angular ASAR imagery in the Watershed Allied Telemetry Experimental Research (WATER). Hydrol. Earth Syst. Sci. 15, 1415–1426.
Wegmüller, U., Santoro, M., Mattia, F., Balenzano, A., Satalino, G., Marzahn, P., Fischer, G., Ludwig, R., Floury, N., 2011. Progress in the understanding of narrow directional microwave scattering of agricultural fields. Remote Sens. Environ. 115, 2423–2433.
Wickel, A., Jackson, T., Wood, E., 2001. Multitemporal monitoring of soil moisture with RADARSAT SAR during the 1997 Southern Great Plains hydrology experiment. Int. J. Remote Sens. 22, 1571–1583.
Ye, N., Walker, J., Wu, X., Jackson, T., Renzullo, L., Merlin, O., Rüdiger, C., Entekhabi, D., DeJeu, R., Kim, E., 2016. In: Towards validation of SMAP: SMAPEX-4 &-5. IEEE, pp. 3469–3472.
Zhang, X., Chen, B., Fan, H., Huang, J., Zhao, H., 2016. The potential use of multi-band SAR data for soil moisture retrieval over bare agricultural areas: hebei, China. Remote Sens. 8, 7.
Zhang, X., Chen, B., Zhao, H., Li, T., Chen, Q., 2018. Physical-based soil moisture retrieval method over bare agricultural areas by means of multi-sensor SAR data. Int. J. Remote Sens. 39, 3870–3890.
Zhu, L., Walker, J.P., Tsang, L., Huang, H., Ye, N., Rüdiger, C., 2019a. Soil moisture

retrieval from time series multi-angular radar data using a dry down constraint. Remote Sens. Environ. 231, 111237.
Zhu, L., Walker, J.P., Ye, N., Rudiger, C., 2016. The effect of radar configuration on effective correlation length. In: Electromagnetics in Advanced Applications (ICEAA), 2016 International Conference on. IEEE, pp. 820–823.
Zhu, L., Walker, J.P., Ye, N., Rüdiger, C., 2019b. Roughness and vegetation change detection: a pre-processing for soil moisture retrieval from multi-temporal SAR imagery. Remote Sens. Environ. 225, 93–106.
Zhu, L., Walker, J.P., Ye, N., Rüdiger, C., Hacker, J., Panciera, R., Tanase, M.A., Wu, X., Gray, D., Stacy, N., Goh, A., Yardley, H., Mead, J., 2018. The Polarimetric L-band Imaging Synthetic aperture radar (PLIS): description, calibration and cross-validation. Ieee Journal of Selected Topics in Applied Earth Observations and Remote Sensing 11, 4513–4525.
Zribi, M., Dechambre, M., 2003. A new empirical model to retrieve soil moisture and roughness from C-band radar data. Remote Sens. Environ. 84, 42–52.
Zribi, M., Gorrab, A., Baghdadi, N., 2014a. A new soil roughness parameter for the modelling of radar backscattering over bare soil. Remote Sens. Environ. 152, 62–73.
Zribi, M., Gorrab, A., Baghdadi, N., Lili-Chabaane, Z., Mougenot, B., 2014b. Influence of radar frequency on the relationship between bare surface soil moisture vertical profile and radar backscatter. IEEE Geosci. Remote Sens. Lett. 11, 848–852.
Zribi, M., Muddu, S., Bousbih, S., Al Bitar, A., Tomer, S.K., Baghdadi, N., Bandyopadhyay, S., 2019. Analysis of L-band SAR data for soil moisture estimations over agricultural areas in the tropics. Remote Sens. 11, 1122.
Zribi, M., Saux-Picart, S., André, C., Descroix, L., Ottlé, C., Kallel, A., 2007. Soil moisture mapping based on ASAR/ENVISAT radar data over a Sahelian region. Int. J. Remote Sens. 28, 3547–3565.
Zribi, M., Taconet, O., Ciarletti, V., Vidal-Madjar, D., 2002. Effect of row structures on radar microwave measurements over soil surface. Int. J. Remote Sens. 23, 5211–5224.